NEWS AND VIEWS

Journal of Semiconductors
(2019) 40, 100401
doi: 10.1088/1674-4926/40/10/100401

Silicon polarization switch based on symmetric polarization splitter-rotators

Defen Guo[1], Kang Hou[2], Weijie Tang[3], and Tao Chu[3,†]

[1]State Key Laboratory on Integrated Optoelectronics, Institute of Semiconductors, Chinese Academy of Sciences, Beijing 100083, China

[2]School of Optoelectronics, Beijing Institute of Technology, Beijing 100081, China

[3]College of Information Science and Electronic Engineering, Zhejiang University, Hangzhou 310027, China

Citation: D F Guo, K Hou, W J Tang, and T Chu, Silicon polarization switch based on symmetric polarization splitter-rotators[J]. *J. Semicond.*, 2019, 40(10), 100401. http://doi.org/10.1088/1674-4926/40/10/100401

1. Introduction

Silicon photonic integration is considered to be one of the most promising techniques in realizing high-density photonic integrated circuits because of its compact device size and CMOS compatible fabrication process. However, due to the large index contrast of silicon waveguides, silicon photonic devices are affected by the large polarization mode dispersion, polarization dependent loss and polarization dependent wavelength characteristics. Polarization transparent circuits and polarization diversity schemes, which have polarization rotators and splitters as common key devices, have been proposed to solve this issue[1–3]. To date, various types of passive polarization rotators have been demonstrated[4–8], all of which are static and operation-fixed. However, the dynamic polarization switch is also needed due to its many applications, including polarization modulation[9, 10], coherent communication[11], quantum computing[12], and polarization diversity[2].

Recently, various dynamic polarization controlling devices based on silicon waveguides have been reported[13–15]. Two kinds of devices can be used to achieve a polarization switch in planar silicon waveguide circuits. The first is a phase modulator whose waveguide is illuminated at 45° of its main axis, as shown in Fig. 1(a). The input light is split into two orthogonal polarizations. With a thermal-optical controlling signal, a phase difference between the two orthogonal polarization states is produced, resulting in a changed output polarization orthogonal to its original state. However, the polarization-dependent phase shifter needs to be long enough because the polarization-dependent thermal optical effect is weak in silicon waveguides. The waveguide length is approximate 700 μm for that with SU8 upper cladding and much longer for that with SiO_2 upper cladding[13]. The second consists of an ordinary polarization splitter rotator (PSR) followed by a series of 3-dB couplers and phase shifters, and a second PSR[15, 16]. This consists of many elements, including at least two PSRs, two 3-dB couplers and one phase shifter to realize polarization switch, as shown in Fig. 1(b). Here, we propose a new design of polarization switch, which consists of one phase shifter and two symmetric PSRs as shown in Fig. 1(c). The symmetric PSR utilizes the linear combination of TE0 and TM0 as orthogonal bases, while the common PSR directly utilizes the TE0 and TM0 as orthogonal bases[17]. Simulation results show that the device has a TM0-to-TE0 polarization extinction ratio of better than 30 dB over the C band. The simplified device has a shorter length of less than 300 μm compared with those previously reported.

2. Design and simulation

The operation principle of the polarization switch can be mathematically explained with transfer matrix method. Without regarding to the insert loss, the Jones' matrix of the symmetric PSR could be expressed as

$$T_1 = \frac{1}{\sqrt{2}}\begin{bmatrix} 1 & e^{j\varphi} \\ 1 & -e^{j\varphi} \end{bmatrix}, \tag{1}$$

in which φ is a parameter related to the structure. The transmission of the phase shifter could be expressed as

$$T_2 = \begin{bmatrix} e^{j\theta} & 0 \\ 0 & 1 \end{bmatrix}, \tag{2}$$

in which θ is the phase difference between the two arms. If the input is TM0 light, the output of the polarization switch can be expressed as the following:

$$T_1^{-1}T_2T_1\begin{bmatrix} 0 \\ 1 \end{bmatrix} = \frac{1}{2}\begin{bmatrix} e^{j\varphi}(e^{j\theta}-1) \\ e^{j\theta}+1 \end{bmatrix}. \tag{3}$$

Giving $\varphi = 0$, we can calculate the relative amplitude and

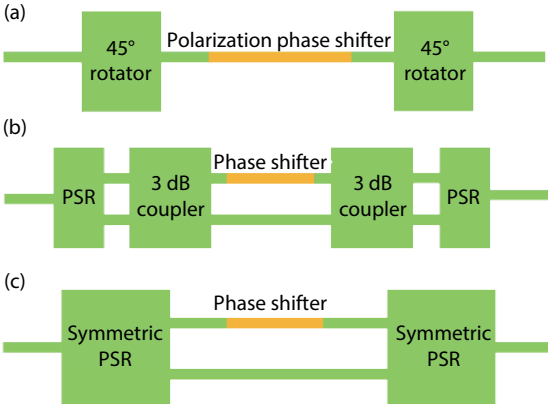

Fig. 1. (Color online) Three kinds of silicon polarization switch

† Correspondence to: T Chu, chutao@zju.edu.cn

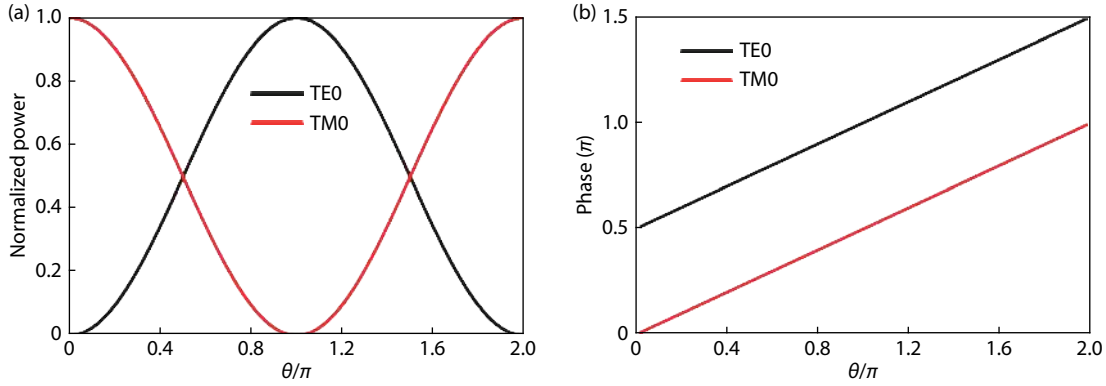

Fig. 2. (Color online) (a) The theoretical relative amplitude and (b) phase of output TE0 and TM0 polarization state when TM0 polarization state is input.

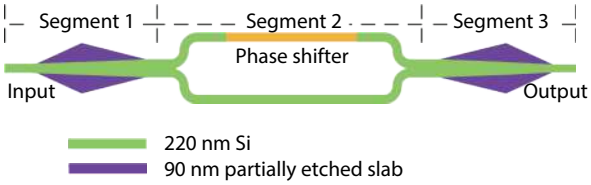

Fig. 3. (Color online) Schematic of the polarization switch, which is designed on a silicon-on-insulator substrate with a 220-nm-high waveguide.

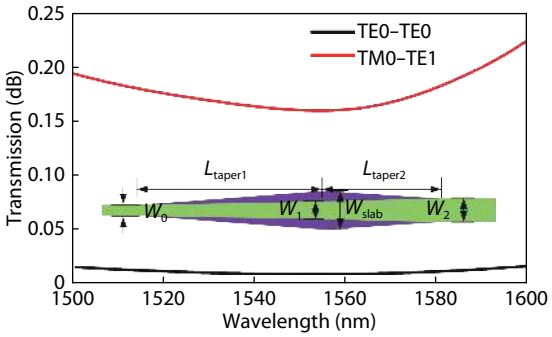

Fig. 4. (Color online) Simulated TM0–TE1 and TE0–TE0 insert loss of the bilevel taper. The insets are the bilevel taper structure comprising rib waveguide with 90-nm-high slab.

phase between the output TE0 light and TM0 light changing with the value of θ, as shown in Fig. 2. We see that the polarization switch can realize dynamic amplitude tuning between TE0 and TM0 light via adjustment of the phase shifter, while its relative phase keeps no change.

The structure of the polarization switch is shown in Fig. 3. For the convenience of design and performance analysis, the switch is divided into three segments. Segment 1 is a bilevel-tapered TM0–TE1 mode converter that converts the input TM0 mode to TE1 mode, while the input TE0 mode keeps unchanged[18]. Segment 2 is a tunable Mach–Zehnder interference (MZI)-type TE1–TE0 mode converter, which consists of a symmetric two-mode *Y* branch acting as a splitter, a pair of arms with a phase shifter, and an inverse two-mode *Y* branch acting as a combiner. The two-mode *Y* splitter divides the input TE1 light into two TE0 light beams with π phase difference, while it splits the input TE0 light into two TE0 with the same phase[19]. The two arms with the phase shifter adjust the phase difference of the propagating light. Subsequently, upon passing the two-mode Y combiner, the two TE0 light beams with π phase difference are combined to TE1 light, whereas the two TE0 light beams with the same phase are combined to TE0 light. Segment 3 is an inverse bilevel-tapered TM0–TE1 mode converter. It converts the input TE1 light to TM0 mode and allows the input TE0 light pass with no change. The polarization switch was designed based on a silicon-on-insulator substrate with a 220-nm-thick top silicon layer. Its basic segments were optimized separately using a 3D finite-difference time-domain (FDTD) simulation tool (Lumerical FDTD solution)[20].

The goal of the bilevel taper design is to balance the device size and the conversion efficiency. As shown in Fig. 4, the width of the input single mode waveguide is set to W_0 = 0.4 μm, while the output two-mode waveguide has width W_2 = 0.8 μm. The height of the slab waveguide is set to 90 nm, which breaks the waveguide vertical symmetry for mode transformation, and it has width W_{slab} = 1.6 μm. Simulated results show that the hybrid TE1 and TM0 modes are generated at a waveguide with a width of approximately 0.48 μm. To obtain a higher conversion efficiency and a smaller footprint, we divide the taper into two parts. The end-width of the first part is set to W_1 = 0.6 μm. The first part is relatively long, so as to yield higher conversion efficiency, with L_{taper1} = 40 μm. The second part is relatively short for reduced device size, with L_{taper2} = 30 μm. The insert loss (IL) is found to be less than 0.25 dB for TM0 and 0.025 dB for TE0 over a wavelength range of 1500–1600 nm, as shown in Fig. 4.

The tunable MZI-type TE1–TE0 mode converter is shown in Fig. 3, which achieves light mode conversion based on the phase difference set between the two MZI arms. The yellow part in Fig. 3 represents a 100-μm-long adjustable phase shifter, which can be controlled through thermo-optical effect. Fig. 5(a) shows that the output light-mode composition varies with the index and temperature increment of the phase shifter and at 1550 nm, according that the thermo-optic coefficient of silicon is 1.86×10^{-4} K^{-1}[21]. The input TE1 light is totally transformed to the TE0 mode at an index (temperature) increment of 0.007 (37.66 K). Furthermore, when the index (temperature) increment is set to 0 or 0.014 (0 or 75.32 K), the input TE1 light passes through the device unchanged. From Fig. 5(b), it can be determined that the TE1-to-TE0 conversion efficiency is more than 95% over a

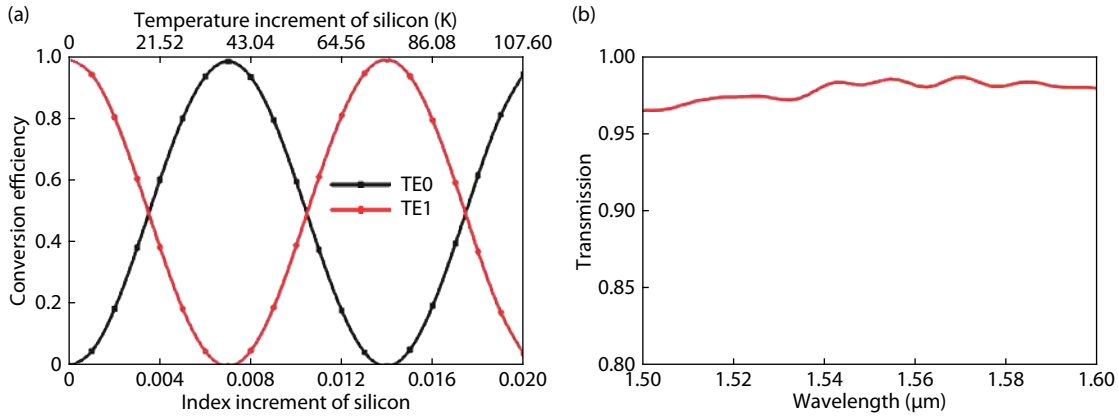

Fig. 5. (Color online) (a) Simulated output light-mode composition of the MZI-type mode converter versus the index and temperature increment of the phase shifter.

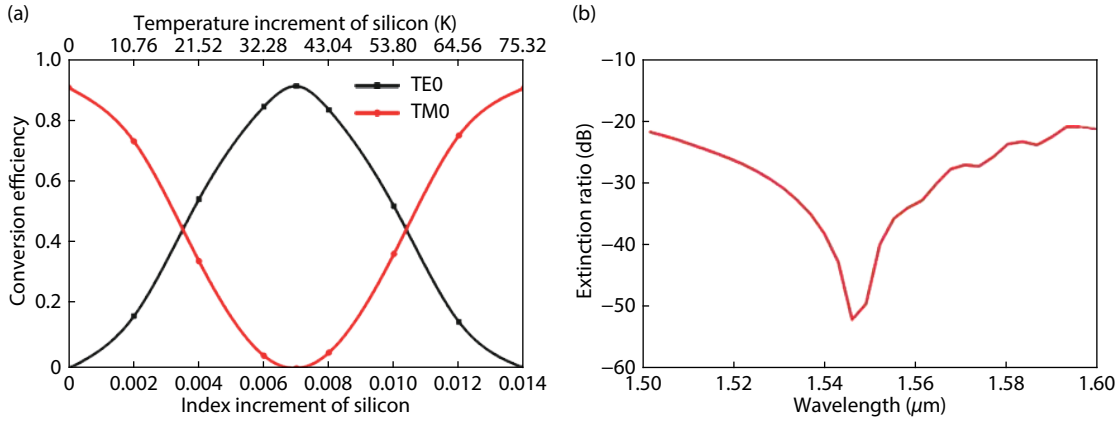

Fig. 6. (Color online) (a) Simulated output polarization state composition of the polarization switch versus the index and temperature increment of the phase shifter with TM0 light input. (b) Simulated TM0–TE0 polarization extinction ratio at index increment (temperature) of 0.007 (37.66 K).

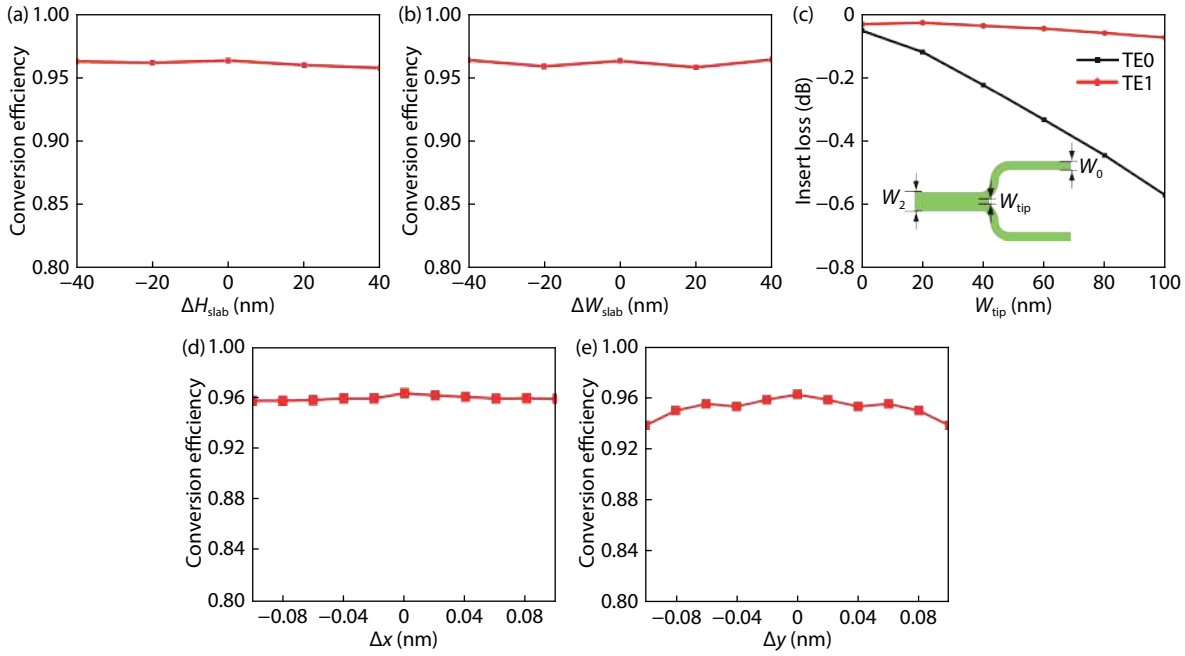

Fig. 7. (Color online) Conversion efficiency of the bilevel taper at 1550-nm versus (a) the fabrication error of the slab height and (b) the slab width . (c) Insert loss of the Y branch for TE0 and TE1. (d) The horizontal and (e) vertical misalignment accuracy of the bilevel taper at 1550 nm.

wavelength range of 1500–1600 nm at an index (temperature) increment of 0.007 (37.66 K).

Using a polarization switch composed of optimized segments, we estimated the overall device performance. The in-

put was set to TM0 light. Fig. 6(a) shows that the output light-polarization composition varies with the index and temperature increment of the phase shifter at 1550 nm. In agreement with the MZI-type mode converter, the TM0 polarization state is totally rotated to TE0 polarization at an index (temperature) increment of 0.007 (37.66 K). The polarization extinction ratio (ER) were calculated, which is defined as ER = 10 × lg ($P_{out,TM0}/P_{out,TE0}$), where $P_{out,TE0}$ and $P_{out,TM0}$ are the output powers of the TE0 and TM0 polarization state, respectively. As shown in Fig. 6(b), the ER is larger than 30 dB over the 1530–1565-nm wavelength. At 1546-nm wavelength, the ER is even larger than 50 dB. The central wavelength with the highest ER can be adjusted by altering phase-shifter index (temperature), which facilitates flexible use.

Fabrication tolerance analysis has to be done for future fabrication. Figs. 7(a) and 7(b) show the TM0-to-TE1 conversion efficiency of the bilevel taper versus the offset of the width and height of the slab waveguide, respectively. The conversion efficiency remains over 95% at 1550-nm wavelength in the range +/− 40 nm. As for the sharp corner of *Y* branch, the insert loss for both TE0 and TE1 is less than 0.6 dB if the width of the corner is within 100 nm, as shown in Fig. 7(c). The 100-nm gap can be fabricated by the electron beam lithography and the 193-nm immersion lithography. The upper cladding material of our device is SiO_2, which is compatible with metal back-end-of-line processes. The horizonal and vertical alignment accuracy for the bilevel taper have been investigated and the simulated results are shown in Figs. 7(d) and 7(e), respectively. The conversion efficiency has almost no deterioration when the misalignment between the slab and the ridge is ±100 nm.

3. Conclusion

We have proposed a silicon polarization switch based on symmetric PSRs. The switch can realize arbitrary polarization amplitude tuning between TE0 and TM0 light. The structure of the device is straightforward and the tuning control is quite simple. The simulated TM0-TE0 polarization extinction ratio is larger than 30 dB over C band. The proposed tunable polarization rotator presents a promising approach to solve the key issue of dynamic polarization control in silicon photonic circuits. Future work can be done to design a device to realize arbitrary polarization state control in silicon photonic circuits.

Acknowledgments

This work was supported by the National Key Research and Development Program of China (No. 2016YFB0402505) and the National Science Foundation of China (NSFC) (No. 61575189 and No. 61635011).

References

[1] Barwicz T, Watts M R, Miloš A. P, et al. Polarization-transparent microphotonic devices in the strong confinement limit. Nat Photonics, 2007, 1(1), 57

[2] Fukuda H, Yamada K, Tsuchizawa T, et al. Ultrasmall and wideband polarization rotator based on silicon wire waveguides. Opt Express, 2007, 16(4), 2628

[3] Dai D, Liu L, Gao S, et al. Polarization management for silicon photonic integrated circuits. Laser Photonics Rev, 2013, 7(3), 303

[4] Ding Y, Ou H, Peucheret C. Wideband polarization splitter and rotator with large fabrication tolerance and simple fabrication process. Opt Lett, 2013, 38(8), 1227

[5] Xiong Y, Wangüemert-Pérez J G, Xu D X, et al. Polarization splitter and rotator with subwavelength grating for enhanced fabrication tolerance. Opt Lett, 2014, 39(24), 6931

[6] Wang J, Niu B, Sheng Z, et al. Novel ultra-broadband polarization splitter-rotator based on mode-evolution tapers and a mode-sorting asymmetric Y-junction. Opt Express, 2014, 22(11), 13565

[7] Guan H, Ma Y, Shi R, et al. Ultracompact silicon-on-insulator polarization rotator for polarization-diversified circuits. Opt Lett, 2014, 39(16), 4703

[8] Liu L, Ding Y, Yvind K, et al. Efficient and compact TE–TM polarization converter built on silicon-on-insulator platform with a simple fabrication process. Opt Lett, 2011, 36(7), 1059

[9] Alferness R C, Buhl L L. High-speed waveguide electro-optic polarization modulator. Opt Lett, 1982, 7(10), 500

[10] Bull J D, Jaeger N A F, Kato H, et al. 40-GHz electro-optic polarization modulator for fiber optic communications systems. Photonics North 2004: Optical Components and Devices, 2004, 5577, 133

[11] Pfau T, Peveling R, Hauden J, et al. Coherent digital polarization diversity receiver for real-time polarization-multiplexed QPSK transmission at 2.8 Gb/s. IEEE Photonics Technol Lett, 2007, 19(24), 1988

[12] Corrielli G, Crespi A, Geremia R, et al. Rotated waveplates in integrated waveguide optics. Nat Commun, 2014, 5, 4249

[13] Alonso-Ramos C, Halir R, Ortega-Moñux A, et al. Highly tolerant tunable waveguide polarization rotator scheme. Opt Lett, 2012, 37(17), 3534

[14] Xu Q, Chen L, Wood M G, et al. Electrically tunable optical polarization rotation on a silicon chip using Berry's phase. Nat Commun, 2014, 5, 5337

[15] Sacher W D, Barwicz T, Taylor B J F, et al. Polarization rotator-splitters in standard active silicon photonics platforms. Opt Express, 2014, 22(4), 3777

[16] Moller L. WDM polarization controller in PLC technology. IEEE Photonics Technol Lett, 2001, 13(6), 585

[17] Ma Y, Liu Y, Guan H, et al. Symmetrical polarization splitter/rotator design and application in a polarization insensitive WDM receiver. Opt Express, 2015, 23(12), 16052

[18] Dai D, Tang Y, Bowers J E. Mode conversion in tapered submicron silicon ridge optical waveguides. Opt Express, 2012, 20(12), 13425

[19] Love J D, Riesen N. Single-, few-, and multimode Y-junctions. J Lightwave Technol, 2012, 30(3), 304

[20] https://www.lumerical.com/

[21] Cocorullo G, Della Corte F G, Rendina I. Temperature dependence of the thermo-optic coefficient in crystalline silicon between room temperature and 550 K at the wavelength of 1523 nm. Appl Phys Lett, 1999, 74(22), 3338